Mixed Poisson distributions in exact solutions of stochastic autoregulation models

Srividya Iyer-Biswas*
James Franck Institute, University of Chicago, Chicago, Illinois 60637, USA

C. Jayaprakash
Department of Physics, The Ohio State University, Columbus, Ohio 43210, USA
(Received 3 April 2012; published 13 November 2014)

In this paper we study the interplay between stochastic gene expression and system design using simple stochastic models of autoactivation and autoinhibition. Using the Poisson representation, a technique whose particular usefulness in the context of nonlinear gene regulation models we elucidate, we find exact results for these feedback models in the steady state. Further, we exploit this representation to analyze the parameter spaces of each model, determine which dimensionless combinations of rates are the shape determinants for each distribution, and thus demarcate where in the parameter space qualitatively different behaviors arise. These behaviors include power-law-tailed distributions, bimodal distributions, and sub-Poisson distributions. We also show how these distribution shapes change when the strength of the feedback is tuned. Using our results, we reexamine how well the autoinhibition and autoactivation models serve their conventionally assumed roles as paradigms for noise suppression and noise exploitation, respectively.

DOI: 10.1103/PhysRevE.90.052712 PACS number(s): 87.10.Mn, 87.10.Ca, 87.16.A−, 87.16.dj

I. INTRODUCTION

Stochastic fluctuations in the numbers of key biochemicals may be significant compared to their mean levels. Such fluctuations arise even in a population of cells that were initially identical due to the inherently probabilistic nature of chemical reactions and the small numbers of reactants involved in key cellular processes such as gene activation, transcription, and translation [1,2]. Consequently, there may be significant cell-to-cell variability of gene products, in particular, protein numbers. Stochastic gene expression and, specifically, such intrinsic fluctuations in protein numbers have been the focus of several experimental and theoretical studies [1–9]. Biologically, the fluctuations in the number of a given protein could be either desirable or detrimental, and thus requiring suppression, for the relevant cellular function [10]. An important system biological goal is to understand how the noise characteristics associated with a given gene regulatory network inform the biological function of the corresponding protein.

Previous studies have indicated that tight control of protein numbers, when desired, is often achieved by an autorepression motif of gene expression [11–15]. It has even been argued that the reason why this network motif occurs far more frequently in nature (40% of the known transcription factors in *E. Coli* are controlled by negative autoregulation [16]) than in studies of randomized networks is because it achieves stability against fluctuations [17]. On the other hand, bimodal distributions of protein numbers may be exploited by cells to dynamically switch between different expression states; this is especially useful for cellular processes where conditional locking of subpopulations of cells into distinct fates needs to be achieved without changing the underlying network structure. The autoactivation motif has been implicated in systems in which such tunable population heterogeneity is desirable [18–21].

Here we explore the interplay between stochastic gene expression and system design by examining two simple stochastic gene pulsing models with autoregulation. It is now well established that many genes transcribe and/or translate in bursts, i.e., mRNA or proteins are produced with significantly varying dead times in between successive rounds of production [2,3,8,22,23]. This important aspect of gene expression is encapsulated in a model in which the gene can stochastically switch between long-lived off states and on states leading to intermittent mRNA and protein expression. (We prefer the term pulsing to bursting since the latter terminology could be misleading [22].) Therefore, in the positive (negative) feedback model considered here, the amount of protein produced is assumed to proportionally increase the propensity of the gene to dwell in the on (off) states.

We use the Poisson representation, first introduced in [24], a technique whose particular usefulness in the context of analyzing feedback models of gene expression we elucidate here. While models of stochastic gene expression, including those for autoregulation, have been previously considered [7,8,22,23,25,26], what has been lacking is a systematic prescription for classifying where in the multidimensional parameter space of each model qualitatively distinct distributions are obtained. Typical solutions and examinations of these models utilize the generating function method to solve the corresponding master equation or numerical simulations based on the exact Gillespie algorithm or combinations thereof. However, in both these approaches, systematically classifying the entire parameter space of the model is not feasible in general. Here we show how such a classification is possible when the physically well-motivated Poisson representation is instead used, since it naturally yields the particular dimensionless combinations of parameters that are the important ones for each model. We use this representation to both derive

*iyerbiswas@uchicago.edu

the exact steady-state protein distributions in the two models considered here and also analyze the respective parameter spaces, demarcating where in them bimodal, power-law-tail, sub-Poissonian, and other distributions occur. Using the classification of allowed distributions, we then reexamine how well the models of negative and positive feedback considered here serve their conventional roles as paradigms for noise suppression and noise exploitation, respectively.

While the idea of writing down protein distributions as exact linear superpositions of Poisson distributions is relatively new [8], mixtures of Poisson distributions have been long studied in various contexts including photon statistics in quantum optics [27] and in accident proneness models in actuarial sciences [28]. Remarkably, in both the autoactivation and the autorepression cases, we find classes of mixed Poisson distributions [29]. Moreover, they arise *dynamically* in these models. We also show that the beta-Poisson mixture, which has been previously utilized as a versatile prior distribution in accident proneness models [28], naturally arises as a limiting case from these dynamics.

II. THEORETICAL FRAMEWORK

A. Poisson representation

Detailed expositions of the Poisson representation can be found in [24,28,30]. We have briefly discussed application of the Poisson representation to linear models of gene regulation without feedback in [8]. Here we analyze how the exact steady-state protein distributions $P(p)$ of the models with feedback, positive or negative, may be represented as a superposition of Poisson distributions, with a weighting probability density $\rho(\lambda)$ for the Poisson mean λ. In other words, we determine whether a probability density $\rho(\lambda)$ can be found such that

$$P(p) = \int_0^\infty \frac{e^{-\lambda}\,\lambda^p}{p!}\rho(\lambda)\,d\lambda. \tag{1}$$

If indeed such a probability density $\rho(\lambda)$ can be found, an immediate implication is that the corresponding $P(p)$ must be super-Poissonian, i.e., its variance must be greater than its mean, and thus the ratio of the two, the Fano factor (FF) $\mathcal{F}$, must be greater than unity. (In contrast, the Poisson distribution has variance equal to mean and thus an FF equal to 1.)

The superposing or mixing density $\rho(\lambda)$ is a function of a continuous variable λ. In contrast, $P(p)$ is a function of p, which is only allowed discrete (positive integer) values. Thus the convexity and monotonicity properties of $\rho(\lambda)$ are easier to ascertain than that for $P(p)$. In turn, these properties determine the allowed shapes of $P(p)$ for a given stochastic gene expression model. Specifically, bimodal $P(p)$ distributions correspond to concave (upward) $\rho(\lambda)$; power-law tails in $P(p)$ arise when $\rho(\lambda)$ itself has a monotonically decreasing power-law tail; a monotonically increasing $\rho(\lambda)$ leads to a unimodal $P(p)$ distribution with the mode approximately at the upper edge of the λ interval; when $\rho(\lambda)$ is concave downward with a maximum at some intermediate value of λ, then unimodal $P(p)$ distributions with a mode around the same value result. We use the exact, analytical expressions that we derive for $\rho(\lambda)$, to map out where in the parameter space each qualitatively distinct shape of $P(p)$ arises.

B. Master equations for the autoactivation and autorepression models

1. Autoactivation

The autoactivation model considered here is given by the following reactions, with the protein switching the gene from the off to the on state:

$$\begin{aligned} D &\underset{c_b}{\overset{c_f}{\rightleftharpoons}} D^*, \\ D + P &\xrightarrow{a} D^* + P, \\ D^* &\xrightarrow{p_b} D^* + P, \\ P &\xrightarrow{p_d} \emptyset\,. \end{aligned} \tag{2}$$

We use $P_0(p,t)$ and $P_1(p,t)$ to denote the probabilities that there are p proteins at time t and that the gene is in the off and on state, respectively. The master equations for the time evolution of these probabilities are then obtained using standard techniques [30]. They are

$$\begin{aligned} \frac{dP_0(p,t)}{dt} &= -c_f P_0(p,t) + c_b P_1(p,t) - ap P_0(p,t) \\ &\quad + p_d[(p+1)P_0(p+1,t) - pP_0(p,t)], \\ \frac{dP_1(p,t)}{dt} &= c_f P_0(p,t) - c_b P_1(p,t) + ap P_0(p,t) \\ &\quad + p_d[(p+1)P_1(p+1,t) - pP_1(p,t)] \\ &\quad + p_b[P_1(p-1,t) - P_1(p,t)]. \end{aligned} \tag{3}$$

We define $\rho_0(\lambda)$ and $\rho_1(\lambda)$ as

$$P_\alpha(p,t) \equiv \int_0^\infty d\lambda\,\rho_\alpha(\lambda,t)e^{-\lambda}\frac{\lambda^p}{p!} \quad \text{for} \quad \alpha = 0 \text{ or } 1 \tag{4}$$

and note that $\rho(\lambda) = \rho_0(\lambda) + \rho_1(\lambda)$ satisfies the normalization condition $\int d\lambda\,\rho(\lambda) = 1$. The corresponding master equations for $\rho_\alpha(\lambda)$ are then given by

$$\begin{aligned} \partial_t \rho_0(\lambda,t) &= -c_f \rho_0(\lambda,t) + c_b \rho_1(\lambda,t) + \partial_\lambda[\lambda\rho_0(\lambda,t)] \\ &\quad - a[\lambda\rho_0 - \partial_\lambda(\lambda\rho_0)], \\ \partial_t \rho_1(\lambda,t) &= c_f \rho_0(\lambda,t) - c_b \rho_1(\lambda,t) + \partial_\lambda[\lambda\rho_1(\lambda,t)] \\ &\quad + a[\lambda\rho_0 - \partial_\lambda(\lambda\rho_0)] - p_b \partial_\lambda \rho_1(\lambda,t), \end{aligned} \tag{5}$$

with the boundary condition

$$\pm\, a e^{-\lambda}\frac{\lambda^p}{p!}\lambda\rho_0(\lambda)\Big|_0^{\lambda_{\max}} = 0 \tag{6}$$

for $0 \leqslant \lambda \leqslant \lambda_{\max}$; $\lambda_{\max}$ needs to be computed. In going from Eq. (3) to Eq. (5) we have imposed the condition that the boundary terms resulting from integration by parts vanish. The solution we obtain does indeed behave as required and so the assumption that the boundary terms vanish can be justified *a posteriori* (see Sec. III).

2. *Autorepression*

The autorepression model considered here is given by the reactions

$$\begin{aligned} D &\underset{c_b}{\overset{c_f}{\rightleftharpoons}} D^*, \\ D^* + P &\xrightarrow{r} D + P, \\ D^* &\xrightarrow{p_b} D^* + P, \\ P &\xrightarrow{p_d} \emptyset. \end{aligned} \tag{7}$$

We can derive the master equations satisfied by the λ densities as before,

$$\begin{aligned} \partial_t \rho_0(\lambda,t) &= -c_f \rho_0(\lambda,t) + c_b \rho_1(\lambda,t) + \partial_\lambda[\lambda \rho_0(\lambda,t)] \\ &\quad + r[\lambda \rho_1 - \partial_\lambda(\lambda \rho_1)], \\ \partial_t \rho_1(\lambda,t) &= c_f \rho_0(\lambda,t) - c_b \rho_1(\lambda,t) + \partial_\lambda[\lambda \rho_1(\lambda,t)] \\ &\quad - r[\lambda \rho_1 - \partial_\lambda(\lambda \rho_1)] - p_b \partial_\lambda \rho_1(\lambda,t), \end{aligned} \tag{8}$$

with the boundary condition

$$-e^{-\lambda}(p_b - \lambda - r\lambda)\frac{\lambda^p}{p!}\rho_1(\lambda)\Big|_0^{\lambda_{\max}} = 0 \tag{9}$$

for $0 \leqslant \lambda \leqslant \lambda_{\max}$, where such a $\lambda_{\max}$ must be found.

III. RESULTS

To place our results for the autoactivation and autorepression models in context, we will find it useful to compare these results with those derived for the linear pulsing model in [8]. Both autoregulation models reduce to the linear pulsing model (LPM) in the limit where the autoactivation strength a or the autorepression strength r tends to 0. In [8] we have also shown how the phase diagram of all possible distributions for the LPM can be classified in terms of the two rescaled dimensionless rates c_f/p_d and c_b/p_d.

A. Autoactivation

The coupled master equations (5) can be solved using standard techniques and give

$$\rho(\lambda) = \mathcal{N} e^{[a/(p_d+a)]\lambda} \lambda^{c_f/(p_d+a)-1}\left(\frac{p_b}{p_d} - \lambda\right)^{c_b/(p_d+a)-1}, \tag{10}$$

with $0 \leqslant \lambda \leqslant p_b/p_d$; $\mathcal{N}$ is the normalization constant. The choice of $\lambda_{\max} = p_b/p_d$ ensures that the boundary terms vanish, as required. This exact expression leads naturally to the correct parametrization of the combinations of the rate constants that are relevant for analyzing this nonlinear model. We rescale λ by p_b/p_d so that it lies between 0 and 1. It is useful to rescale all rates by the effective protein degradation rate p_d. For convenience in classifying the different kinds of protein distributions that arise in this model, we define the following parameters: $\alpha \equiv a\, p_b/(1+a)$, $\phi \equiv c_f/(1+a)$, and $\beta \equiv c_b/(1+a)$. We then have

$$\rho(\lambda) = \mathcal{N} e^{\alpha\lambda} \lambda^{\phi-1}(1-\lambda)^{\beta-1}. \tag{11}$$

Note that ϕ and β characterize the singularity at the upper and lower limits of λ. Using this superposition of the Poisson representation, we have found that in each of the four quadrants determined by ϕ and β greater than or less than 1, the protein distribution has a distinct shape. Since the superposing density $\rho(\lambda)$ is found to extend from $\lambda = 0$ to $\lambda = p_b$, $P(p)$ extends until $\sim p_b$. When the density diverges at both limits, i.e., ϕ and $\beta < 1$, yielding a ρ that is concave upward, the protein distribution is bimodal. When ρ vanishes at both limits, i.e., ϕ and $\beta > 1$, yielding a ρ that is concave downward, a broad bell-shaped distribution of proteins arises.

As the autoactivation strength $a \to 0, \alpha \to 0, \phi \to c_f$, and $\beta \to c_b$ the protein distribution of the autoactivation model becomes the exact steady-state distribution [8] obtained in the LPM. The latter is a beta distribution

$$\rho(\lambda) = \mathcal{N} \lambda^{c_f-1}(1-\lambda)^{c_b-1}. \tag{12}$$

Thus, the phase diagram of possible distributions in this model is very similar, in large regions of the parameter space ϕ and β, to that of the LPM, despite the autoactivation, once we identify ϕ and β in this model with c_f and c_b in the simple pulsing model.

We focus on the most interesting feature that arises in this phase diagram in this model. Consider the quadrant where $\phi < 1$ and $\beta > 1$. When $a = 0$, i.e., in the LPM, we have found [8] long-tail distributions with power-law behavior. In the autoactivation model, in contrast, two possibilities arise depending on whether α is less than or greater than $\alpha_c \equiv (\sqrt{1-\phi} + \sqrt{\beta - 1}\,)^2$. In the former case long-tail distributions with power-law regions arise, with an exponent $\phi - 1$ as in the $a = 0$ case.

For $\alpha > \alpha_c$ the distribution becomes an unusually behaved bimodal distribution. To appreciate its nature we recall that when both ϕ and β are less than 1 (Fig. 1) bimodal distributions occur with the two modes always at 0 and p_b, i.e., at the edges of the allowed values of λ. As a the activation strength increases, the weights around 0 and p_b are redistributed without affecting the separation between the modes. This is the classic binary response [18] typically associated with autoactivation: Cells may be thought to be divided into two subpopulations with low and high protein numbers and increasing activation strength only changes their relative proportions. In contrast, the present bimodal distribution exhibits a second mode not at p_b, the maximum allowed value of λ, but at intermediate values. As α is increased by increasing a, the protein distribution goes from being a monotonically decreasing power law to bimodal because autoactivation affects cells with intermediate numbers of proteins the most. Thus, when the feedback strength is strong enough that $\alpha > \alpha_c$, a new minimum and a new maximum develop in $\rho(\lambda)$, at intermediate values of λ. Correspondingly, $P(p)$ becomes bimodal with the second mode arising at a value of $p < p_b$. As the activation strength increases, this mode tends to higher values of p, but the weight at 0 (the first mode) simultaneously erodes rapidly, making the distribution effectively unimodal for strong enough activation. Thus, in this quadrant, even though bimodal distributions arise for intermediate activation strength, the response to increasing activation is really graded, as illustrated in Fig. 1. As a increases, the protein distribution goes from being negatively skewed, with a large likelihood of obtaining a small number of proteins, to a positively skewed distribution, with a large likelihood of obtaining a large number of proteins.

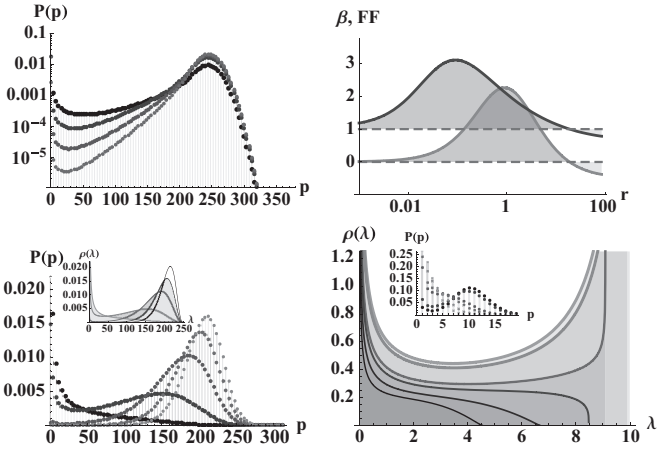

FIG. 1. The top left shows that the response of the protein distribution to increasing activation strength in the $\phi < 1, \beta < 1$ quadrant in the autoactivation model resembles the classic binary response associated with autoactivation systems. The bottom left shows that the effect of increasing activation strength a on the protein distribution in the fourth quadrant ($\phi < 1, \beta > 1$) is graded. The top right shows the effect of increasing autorepression strength r on the Fano factor of the protein distribution in the autorepression model. For the values chosen, both β and the Fano factor go through maximum values at (different) intermediate values of r, before the distribution becomes sub-Poissonian after the threshold value $r = r_0$; this happens exactly when $\beta = 0$. The bottom right shows the effect of increasing autorepression strength r on the protein distribution in the autorepression model. Six different points from the above figure are chosen from the range where β remains positive. The other rates are the same as the ones used in the top right figure. Here r increases from lighter to darker values.

We point out the possible relevance of our results to the observation in an experiment of To and Maheshri [31] of bimodal protein expression in a synthetic yeast system with positive feedback and no cooperativity as in our model. As the activation increases, their distribution goes from a broad bell-shaped distribution to the bimodal distribution similar to the one described above. Our model explains their observation of graded response of the 1xtetO promoter with increasing autoactivation strength. As expected from our model, with increasing a, the mode at larger value travels further towards the right and acquires more weight until a Poisson-like distribution occurs.

Since this model is nonlinear the equations for all the moments are coupled and one needs the full distribution to obtain even the lowest two moments. Using the exact solution for the distribution, one can evaluate the FF, the ratio of the variance to the mean of a distribution. The FF may or may not go through a maximum value as a is increased, but beyond a threshold the FF always decreases with a and tends to 1 as $a \to \infty$. Thus increasing autoactivation results in noise reduction, a role not conventionally associated with positive feedback. This is true since the gene is always on as the activation strength tends to infinity and a Poisson protein distribution with $\mathcal{F} = 1$ results. For any initial choice of parameters, for large enough a, both ϕ and β fall below 1 and the protein distribution becomes bimodal. However, in the limit $a \to \infty$, the mode at 0 is entirely eroded and $\rho(\lambda) \to \delta(p_b - \lambda)$: $P(p)$ becomes Poissonian.

B. Autorepression

The analysis of this model proceeds along the same lines as the autoactivation model. Once again, this formulation leads naturally to the correct parametrization of the combinations of the rate constants that are relevant for analyzing this nonlinear model. We define the parameters $\alpha \equiv r p_b/(1+r)^2$, $\phi \equiv c_f$, and $\beta \equiv p_b r/(1+r)^2 + (c_b - c_f r)/(1+r)$. All rates have been scaled by the protein degradation rate p_d as before. In terms of these variables, the steady state generating function is identical in form to that derived in the autoactivation model.

However, there is a subtle difference that has profound consequences: The parameter β can become *negative* for suitably chosen rates p_b, c_f, c_b, and r in this model, unlike the autoactivation case. Thus the weighting probability density $\rho(\lambda)$ can be found only if $\beta > 0$. This immediately implies that for $\beta > 0$, the protein distribution in the autorepression model is super-Poissonian, i.e., its FF is greater than 1 and thus noisier than the Poisson distribution that arises in the simple birth-death model.

When $\beta < 0$, we find that the protein distribution becomes sub-Poissonian, i.e., its FF becomes less than 1. Thus, only when $\beta < 0$ can the autorepression be said to be strong enough to cause reduction of the noise level in related models, such as the LPM and the autoactivation model. On analyzing the condition $\beta < 0$, we find that for any given value of the rates c_f, c_b, and p_b, there is a threshold value of the repression strength r_0 such that when r increases beyond this threshold value, the distribution becomes sub-Poissonian (as illustrated in Fig. 1). As seen in the top right panel of Fig. 1, this suppression occurs for large values of r and over a narrow range. Exactly at the threshold value, the Fano factor is found to be unity. The expression for r_0 is

$$r_0 = \frac{c_b + p_b - c_f + \sqrt{(c_b + p_b - c_f)^2 + 4 c_f c_b}}{2 c_f}. \quad (13)$$

For values of $r > r_0$, i.e., when the distribution is sub-Poissonian, a formal expression for $\rho(\lambda)$ may be derived, with the understanding that it can no longer be interpreted as a probability density. In fact, λ now extends over the complex plane. Remarkably, even in this case, the functional form of $\rho(\lambda)$ remains the same for a suitably chosen contour. In this case, depending on whether c_f is less than or greater than 1, the protein distribution is a monotonically decreasing or a sharply peaked bell-shaped distribution, respectively.

When $\beta > 0$, we find that the different possible distributions of the autoactivation models all occur for autorepression for appropriate values of α, β, and ν when $\beta > 0$, as illustrated in Fig. 1. This underscores the inadvisability of naively inferring that the choice of autoinhibition motif is designed to obtain noise suppression without further exploring the specific details of the system. See also [32] for a control and information theoretical perspective on the issue. Quantitatively, λ is in the range $0 \leqslant \lambda \leqslant p_b/(1+r)$ and so the protein distribution extends to about $p \sim p_b/(1+r)$. The effective parameter β is now a function of all the rates in the problem while the effective parameter $\phi = c_f$ as in the linear pulsing model.

IV. CONCLUSION

The autoregulation motif is ubiquitous in gene regulation [2,17]. The autoregulation models studied here are admittedly simplified descriptions of those observed in nature: We have not included separate transcription and translation steps. In prokaryotes, since mRNAs are rapidly translated into proteins, this is typically a reasonable approximation. For eukaryotic systems, when the mRNA time scale is significant, these results should not be applied literally. Further, the effects of cooperative autoregulation are not included in our models. However, even in this simple model a plethora of behaviors is observed including power laws and bimodal distributions that behave in a graded fashion and sub-Poissonian statistics. We have also established the utility of the Poisson representation, which yields quite naturally the important, scaled, dimensionless parameters that characterize nonlinear gene regulation models. We have shown that autoactivation produces binary responses to increasing activation strength and that autorepression produces noise-suppressed sub-Poissonian protein distributions in very limited regions of the parameter space. Our work serves to add a note of caution to assuming that positive and negative feedback, when found in natural biological systems, are present to serve these purposes.

ACKNOWLEDGMENTS

C.J. acknowledges support through NIAID Contract No. HHSN272201000054C. S.I.-B. acknowledges useful discussions with N. Maheshri, A. Walczak, N. Wingreen, and R. R. Biswas.

[1] J. Paulsson, Nature (London) **427**, 415 (2004).
[2] A. Raj and A. van Oudenaarden, Cell **135**, 216 (2008).
[3] A. Raj, C. S. Peskin, D. Tranchina, D. Y. Vargas, and S. Tyagi, PLoS Biol. **4**, e309 (2006).
[4] I. Golding, J. Paulsson, S. M. Zawilski, and E. C. Cox, Cell **123**, 1025 (2005).
[5] J. M. Raser and E. K. O'Shea, Science **304**, 1811 (2004).
[6] T. B. Kepler and T. C. Elston, Biophys. J. **81**, 3116 (2001).
[7] J. E. M. Hornos, D. Schultz, G. C. P. Innocentini, J. Wang, A. M. Walczak, J. N. Onuchic, and P. G. Wolynes, Phys. Rev. E **72**, 051907 (2005).
[8] S. Iyer-Biswas, F. Hayot, and C. Jayaprakash, Phys. Rev. E **79**, 031911 (2009).
[9] J. M. Pedraza and J. Paulsson, Science **319**, 339 (2008).
[10] A. Eldar and M. Elowitz, Nature (London) **467**, 167 (2010).
[11] M. Savageau, Nature (London) **252**, 546 (1974).
[12] A. Becskei and L. Serrano, Nature (London) **405**, 590 (2000).
[13] M. Thattai and A. van Oudenaarden, Proc. Natl. Acad. Sci. USA **98**, 8614 (2001).
[14] Y. Dublanche, K. Michalodimitrakis, N. Kummerer, M. Foglierini, and L. Serrano, Mol. Syst. Biol. **2**, 41 (2006).
[15] D. Austin, M. Allen, J. McCollum, R. Dar, J. Wilgus, G. Sayler, N. Samatova, C. Cox, and M. Simpson, Nature (London) **439**, 608 (2006).
[16] D. Thieffry, A. M. Huerta, E. Perez-Rueda, and J. Collado-Vides, Bioessays **20**, 433 (1998).
[17] U. Alon, *An Introduction to Systems Biology: Design Principles of Biological Circuits* (CRC, Boca Raton, 2006).
[18] A. Becskei, B. Seraphin, and L. Serrano, EMBO J. **20**, 2528 (2001).
[19] M. Acar, J. Mettetal, and A. van Oudenaarden, Nat. Genet. **40**, 471 (2008).
[20] W. Smits, C. Eschevins, K. Susanna, S. Bron, O. Kuipers, and L. W. Hamoen, Mol. Microbiol. **56**, 604 (2005).
[21] G. Suel, R. Kulkarni, J. Dworkin, J. Garcia-Ojalvo, and M. B. Elowitz, Science **315**, 1716 (2007).
[22] J. Paulsson, Phys. Life Rev. **2**, 157 (2005).
[23] N. Friedman, L. Cai, and X. S. Xie, Phys. Rev. Lett. **97**, 168302 (2006).
[24] C. Gardiner and S. Chaturvedi, J. Stat. Phys. **17**, 429 (1977).
[25] P. Visco, R. J. Allen, and M. R. Evans, Phys. Rev. Lett. **101**, 118104 (2008).
[26] P. Visco, R. J. Allen, and M. R. Evans, Phys. Rev. E **79**, 031923 (2009).
[27] J. R. Klauder and E. C. G. Sudarshan, *Fundamentals of Quantum Optics* (Dover, New York, 2006).
[28] J. Grandell, *Mixed Poisson Processes* (Chapman & Hall, London, 1997).
[29] D. Karlis and E. Xekalaki, Int. Stat. Rev. **73**, 35 (2005).
[30] C. W. Gardiner, *Handbook of Stochastic Methods*, 2nd ed. (Springer, Berlin, 1997).
[31] T.-L. To and N. Maheshri, Science **327**, 1142 (2010).
[32] I. Lestas, G. Vinnicombe, and J. Paulsson, Nature (London) **467**, 174 (2010).